Batteries & Supercaps

Research Article
doi.org/10.1002/batt.202500230

Chemistry Europe
European Chemical Societies Publishing

www.batteries-supercaps.org

Temperature-Dependent Morphological Evolution of Sn Metal Anode for Aqueous Sn-Ion Batteries

Young-Hoon Lee, Hyeonjun An, Eunbin Park, Yung-Eun Sung,* and Seung-Ho Yu*

There has been growing interest in aqueous batteries, which are considered safer and more cost-effective compared to Li-ion batteries. Among them, aqueous Sn-ion batteries have emerged as promising alternatives because of their high specific capacity and wide voltage window. Despite these numerous advantages, in aqueous-based electrolytes, significant variations in metal growth behavior with temperature lead to severe performance degradation, necessitating a fundamental investigation into the underlying mechanisms to develop high-performance aqueous batteries capable of operating across a wide temperature range. Therefore, this study for the first time examines the temperature-dependent Sn metal plating and stripping behavior in aqueous Sn-ion batteries. The results indicate that, at low temperatures, uneven pits are formed during stripping, leading to a rough and nonuniform surface. These pits serve as nucleation sites for deposition during plating, further exacerbating surface irregularities. In contrast, at high temperatures, stripping occurs uniformly along the grain boundaries and grain surfaces, resulting in a smooth and homogeneous surface. Similarly, plating under high-temperature conditions leads to uniform Sn deposition. In contrast, the corrosion tests reveal that pits form on the electrode surface under high-temperature conditions, leading to deterioration. These findings are expected to contribute to the development of high-performance aqueous Sn-ion batteries.

1. Introduction

Over the past two decades, Li-ion batteries (LIBs) have evolved significantly and have become widely used in a variety of applications, including mobile phones, electric vehicles, power tools, and energy storage systems (ESS). However, the rapid development and widespread use of LIBs have also led to increasing discussions on several challenges, including safety issues. The safety issue associated with LIBs arises from the use of flammable organic solvents in electrolytes, which may result in the emission of toxic gases and potentially cause severe fire hazards under abuse conditions.[1–3] In response to these concerns, aqueous batteries have recently gained significant attention. Among them, aqueous Zn-ion batteries (AZIBs) and Sn-ion batteries (ASIBs) have attracted considerable attention due to their low fire risk, environmental compatibility, and cost-effectiveness.[4–9] The unique electrochemical properties of Sn make it particularly suitable for high-capacity battery applications. Sn offers a high theoretical specific capacity of 451.6 mAh g^{-1}, attributed to its ability to undergo bivalent (Sn^{2+}) redox reactions, and exhibits a wide voltage window of ≈1.8 V when paired with MnO_2 cathodes.[10] Furthermore, Sn remains chemically stable in acidic and alkaline environments, unlike other metal anodes for aqueous batteries such as Fe, Zn, and Ni, which suffer from corrosion and capacity loss.[11–13] Additionally, the body-centered-tetragonal structure of Sn promotes uniform surface energy while guiding anisotropic growth, leading to polyhedral and uniform electrodeposition.[14] Thus, Sn has potential as an advanced metal anode for next-generation high-energy aqueous batteries.

Despite these considerable benefits, achieving stable operation across a wide temperature range remains a critical challenge for the commercialization of aqueous batteries.[15,16] Most aqueous batteries encounter issues at low temperatures due to decreased ionic mobility and increased electrolyte viscosity, resulting in reduced ionic conductivity.[17,18] Conversely, at high temperatures, increased reactivity between electrodes and electrolytes often triggers undesirable side reactions.[19,20] Since temperature influences plating and stripping processes in metal-electrode-based aqueous batteries, including AZIBs and ASIBs,[21,22] in the case of AZIBs, the mechanism of Zn deposition under varying temperatures has already been elucidated. A decrease in temperature has been reported to increase the overpotential during Zn deposition, thereby raising the nucleation energy. This leads to the formation of smaller and denser

Y.-H. Lee, S.-H. Yu
Department of Chemical and Biological Engineering
Korea University
145 Anan-ro, Seoul 02841, Korea
E-mail: seunghoyu@korea.ac.kr

H. An, E. Park, Y.-E. Sung
School of Chemical and Biological Engineering
Seoul National University
1 Gwanak-ro, Seoul 08826, Korea
E-mail: ysung@snu.ac.kr

E. Park, Y.-E. Sung
Center for Nanoparticle Research
Institute for Basic Science (IBS)
1 Gwanak-ro, Seoul 08826, Korea

S.-H. Yu
Department of Battery-Smart Factory
Korea University
145 Anan-ro, Seoul 02841, Korea

Supporting information for this article is available on the WWW under https://doi.org/10.1002/batt.202500230

Research Article
doi.org/10.1002/batt.202500230
Chemistry Europe
European Chemical Societies Publishing

deposits, which can ultimately improve battery performance.[23] However, for ASIBs, the plating and stripping behaviors of Sn under different temperatures have not yet been fully understood.

Therefore, in this study, we investigated the morphological changes of Sn metal anodes under varying temperature conditions. To address this, we examined the electrode morphology under different temperature conditions (0, 25, and 60 °C) at a current density of 1 and 10 mA cm^{-2}. It was observed that elevated temperatures promote uniform plating and stripping behaviors, thereby enhancing the electrochemical performance of ASIBs. However, additional corrosion tests at different temperatures revealed that while a uniform electrode surface was maintained at 0 and 25 °C, pits formed at 60 °C, indicating potential drawbacks. In this study, we aimed to clarify the mechanism of Sn deposition, which could provide insights into the development of high-performance ASIBs.

2. Results and Discussion

To investigate the effect of temperature on the electrode surface during plating and stripping, electrochemical tests were performed with Sn symmetric cells using 0.1 M $SnSO_4$ in 2 M H_2SO_4 as the reference electrolyte. In the first set of experiments, a single-plating process was conducted under three temperature conditions (0, 25, and 60 °C) at a current density of 1 mA cm^{-2} for 1 mAh cm^{-2}. The electrode on which Sn was initially deposited is referred to as the "plated side," whereas the electrode from which Sn was removed during stripping is referred to as the "stripped side." As shown in the voltage profiles in **Figure 1**a, the overpotential during plating exhibited a temperature-dependent trend. Specifically, the overpotential was measured as 6.84 mV at 0, 3.24 mV at 25, and 1.24 mV at 60 °C, demonstrating that higher temperatures led to lower overpotentials. This trend can be attributed to two factors. From a kinetic perspective, elevated

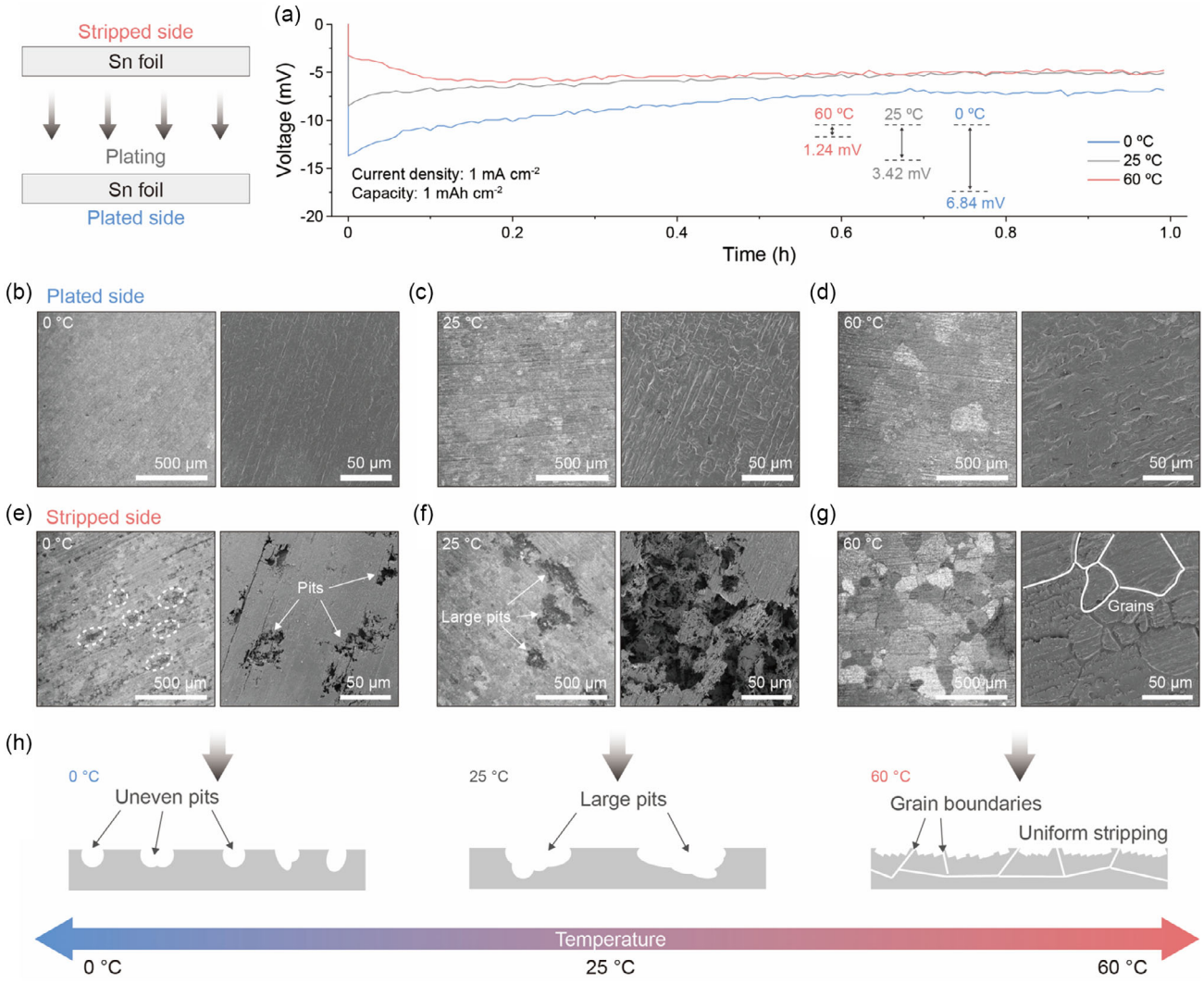

Figure 1. Surface morphology evolution of Sn electrodes during a single-plating process under different temperatures. a) Voltage profiles of Sn symmetric cells at 0, 25, and 60 °C (1 mA cm^{-2} for 1 mAh cm^{-2}). OM and SEM images of the plated side electrodes at b) 0 °C, c) 25 °C, and d) 60 °C. OM and SEM images of the stripped side electrodes after the plating process at e) 0 °C, f) 25 °C, and g) 60 °C. h) Schematic illustration depicting the temperature-dependent stripping behavior of Sn electrodes at a current density of 1 mA cm^{-2}.

temperatures enhance ion mobility, thereby increasing ion conductivity.[24] In addition, the nucleation energy required for the initial Sn deposition decreases at higher temperatures, resulting in a lower plating overpotential.[16] The surface morphology of the plated side electrodes was examined using optical microscope (OM) and scanning electron microscope (SEM). The results revealed uniform plating without noticeable dendrite formation or significant morphological irregularities under all temperature conditions (Figure 1b–d). The uniform surface is attributed to the low plating current density of 1 mA cm^{-2} and the use of identical pristine Sn (bare Sn) electrodes, which help minimize surface variation. In contrast, distinct temperature-dependent morphological differences were observed on the stripped side electrodes (Figure 1e–g). At both 0 and 25 °C, pits were formed, but their size and distribution varied with temperature. At 0 °C, numerous small, uneven pits (1–50 μm) were distributed unevenly across the entire surface. In comparison, at 25 °C, fewer but significantly larger pits (>500 μm) were observed, with several extending deep into the electrode.

Differences in pit morphology are attributed to changes in the stripping behavior at different temperatures. At 0 °C, stripping predominantly occurs at the Sn electrode surface due to the lower ion mobility in the electrolyte, resulting in the widespread formation of small pits.[25] At 25 °C, increased ion mobility promotes stripping both on the Sn surface and at existing pit sites, leading to enlarged pit formation. In contrast, the stripped electrode morphology at 60 °C exhibited different features. Instead of pit formation, distinct grains appeared, which were absent in the bare electrode (Figure S1 and S2, Supporting Information). SEM analysis revealed that Sn was preferentially stripped along grain boundaries, resulting in the formation of gaps between adjacent grains (Figure S3, Supporting Information). Additionally, a layer-by-layer stripping was observed on the grain surfaces, rather than pit formation (Figure S4, Supporting Information). This behavior led to the exposure of grain structures, height differences between adjacent grains, and clear separation between grains due to preferential Sn removal. Stripping predominantly occurs at grain boundaries and grain surfaces under elevated temperature conditions. This behavior is attributed to increased ion mobility, which facilitates selective stripping at highly active sites.[26,27]

X-ray diffraction (XRD) analysis confirmed that the crystallographic structure of the Sn electrodes varied with temperature. At 0 and 25 °C, the (101) plane exhibited a high-intensity peak (Figure S5, Supporting Information). However, at 60 °C, the overall peak intensity was significantly reduced. This can be explained by the similar surface energies of different Sn crystal planes, which facilitate uniform stripping over the entire electrode surface.[28] In summary, under a current density of 1 mA cm^{-2} and a capacity of 1 mAh cm^{-2}, the stripped side electrode surface exhibited distinct temperature-dependent stripping behaviors, leading to noticeable variations in surface morphology (Figure 1h). Stripping at 0 °C generated many small pits across the surface, while at 25 °C, fewer but larger and deeper pits formed. At 60 °C, stripping proceeded uniformly along both grain boundaries and grain surfaces without pit formation.

To examine the influence of temperature under higher current conditions, the current density was raised to 10 mA cm^{-2} while maintaining a constant capacity of 1 mAh cm^{-2}. After a single-plating cycle at 0, 25, and 60 °C, the stripped side electrodes exhibited similar temperature-dependent trends, but with notable differences in pit morphology. At 0 °C, widespread pit formation was again observed, but pits had larger lateral dimensions compared with those formed at lower current densities (**Figure 2**a and S6a, Supporting Information). With the charge capacity fixed at 1 mAh cm^{-2}, lateral pit expansion led to a reduction in stripping depth, indicating that the reaction primarily occurred at the electrode surface. At 25 °C, pit formation appeared more localized, with pits larger in size compared to those observed at 0 °C (Figure 2b and S6b, Supporting Information). Unlike at low current densities, no extremely deep pits were observed. Instead, pits were more widely distributed across the electrode surface (Table S1, Supporting Information). This suggests that at high current densities, ion transport limitations within pits hinder stripping in depth, leading to a more surface-dominated stripping process. At 60 °C, stripping primarily occurred along grain boundaries, similar to the low current density conditions (Figure 2c and S6c, Supporting Information).

On the plated side, distinct plating morphologies were observed under high current density conditions. At 0 °C, the enhanced tip effect led to the formation of numerous small, fern-like dendrites (Figure 2d and S6d, Supporting Information).[29–32] At 25 °C, instead of dendrite formation, polyhedral Sn crystals were deposited as discrete particles (Figure 2e and S6e, Supporting Information). This behavior can be attributed to increased ion mobility at higher temperatures, which mitigates tip effects and promotes more uniform deposition. At 60 °C, plating became even more uniform, without dendrites or polyhedral particles (Figure 2f and S6f, Supporting Information). The edge regions of the plated side exhibited similar trends to the central regions but showed intensified dendrite formation due to the intense electric field at the edges.[33] At 0 °C, fern-like dendrites were denser and longer at the electrode edges than in the central region (Figure 2g and S6g, Supporting Information). At 25 °C, unique square-shaped dendritic structures were observed instead of polyhedral particles (Figure 2h and S6h, Supporting Information). At 60 °C, the plating was mostly uniform, with a few polyhedral particles similar to those observed in the central region at 25 °C. Plating at a high current density of 10 mA cm^{-2} led to more pronounced temperature-dependent morphological changes compared to those observed under low current conditions. Furthermore, the intensified electric field at the edges accelerated dendrite formation. These results indicate that higher temperatures promote more uniform Sn plating and stripping.

Based on these results, further surface changes caused by different surface morphologies were investigated. For this purpose, a single-plating and stripping cycle was performed under each temperature condition. The voltage profile (**Figure 3**a) exhibited a decreasing overpotential trend with increasing temperature, consistent with the results observed in the first set of experiments. No appreciable differences in electrode morphology were detected after the plating–stripping process, regardless of temperature conditions (Figure 3b–d). Furthermore, pits, which were previously observed on electrodes after a single stripping process, were no longer present following a complete plating–

Research Article
doi.org/10.1002/batt.202500230
Chemistry Europe
European Chemical Societies Publishing

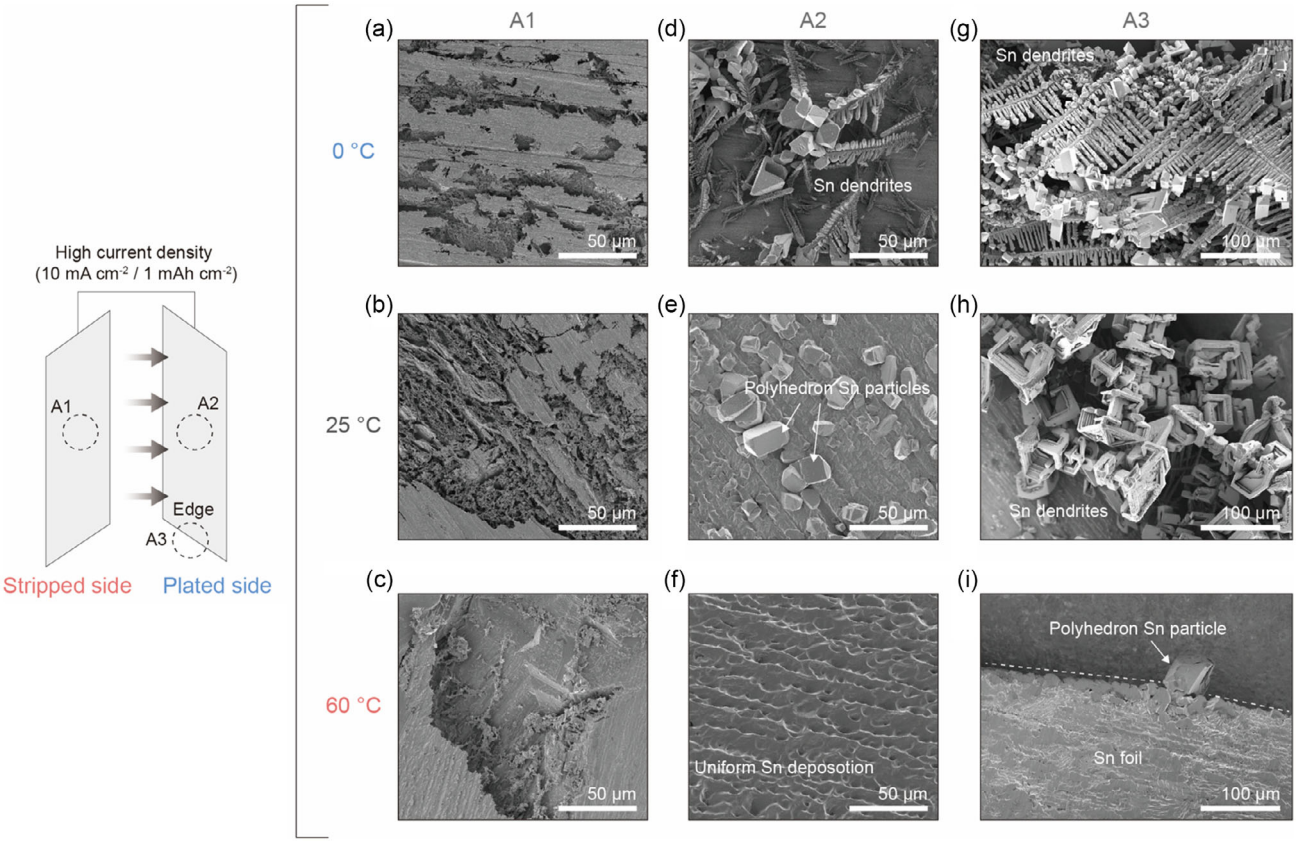

Figure 2. Surface morphology of Sn electrode after a single-plating process at a current density of 10 mA cm^{-2}. SEM images of the stripped side electrodes at a) 0 °C, b) 25 °C, and c) 60 °C. SEM images of the central regions of the plated side electrodes at d) 0 °C, e) 25 °C, and f) 60 °C. SEM images of the edge regions of plated side electrodes at g) 0 °C, h) 25 °C, and i) 60 °C.

stripping cycle. These findings indicate that the initial Sn plating proceeds uniformly, exhibiting no significant temperature-dependent variation. Moreover, during the stripping process, the newly deposited Sn layer is preferentially removed prior to dissolution of the underlying Sn substrate. Temperature-dependent behaviors were clearly evident in the stripping–plating electrodes. This behavior is associated with a localized current concentration around the pits.[34] At 0 °C, the stripped electrodes exhibited small, dispersed pits, which subsequently promoted the formation of small, scattered dendrites on the electrode surface after plating (Figure 3e and S7a, Supporting Information). Similarly, at 25 °C, Sn preferentially deposited within the stripped regions, partially filling the pits and subsequently promoting dendrite growth at the pit sites (Figure 3f and S7b, Supporting Information). The dendrites formed at 25 °C were larger than those observed at 0 °C. This is due to the presence of larger pits at elevated temperatures, which increased the local current density around these sites and consequently accelerated dendrite formation. In contrast, at 60 °C, both stripping and subsequent plating occurred uniformly along grain boundaries and grain surfaces (Figure 3g and S7c, Supporting Information). These observations suggest that the electrode surface morphology is strongly influenced by temperature, resulting in distinct morphological evolution. Specifically, at lower temperatures, nonuniform pits are formed across the electrode surface during stripping, which subsequently act as preferential nucleation sites for dendrite growth during plating. Conversely, at elevated temperatures, the stripping and plating processes proceed uniformly, thereby suppressing dendrite formation (Figure 3h).

Moreover, symmetric coin cells were fabricated to investigate the electrode surface evolution under various temperature conditions (Figure S8a, Supporting Information). Compared to the cell operated at 25 °C, the cell at 0 °C exhibited a higher overpotential during cycling. The cell operated at 60 °C exhibited more stable cycling over a longer period compared to those at 0 and 25 °C. However, the overpotential gradually increased with continued cycling at 60 °C, which is likely associated with progressive oxidation of the electrolyte. As shown in OM images of Sn electrode after 50 cycles, the polyhedral Sn dendrites penetrated the glass fiber separator at 0 and 25 °C, resulting in short circuits (Figure S8b, Supporting Information). However, the electrode surface cycled at 60 °C maintained uniform morphology with defined grain structures, consistent with the previously obtained results. These results demonstrate that finding a way to prevent electrolyte oxidation at high temperatures has the potential to achieve outstanding long-term stability without dendrite growth and increased overpotential at high temperatures.

To further clarify the impact of electrolyte composition and concentration on temperature-dependent Sn deposition behavior, comparative experiments were performed by adjusting the $SnSO_4$ concentration and utilizing an alternative electrolyte based on Sn methanesulfonic acid $(MSA)_2$ in MSA. Specifically, $SnSO_4$

Research Article
doi.org/10.1002/batt.202500230
Chemistry Europe
European Chemical Societies Publishing

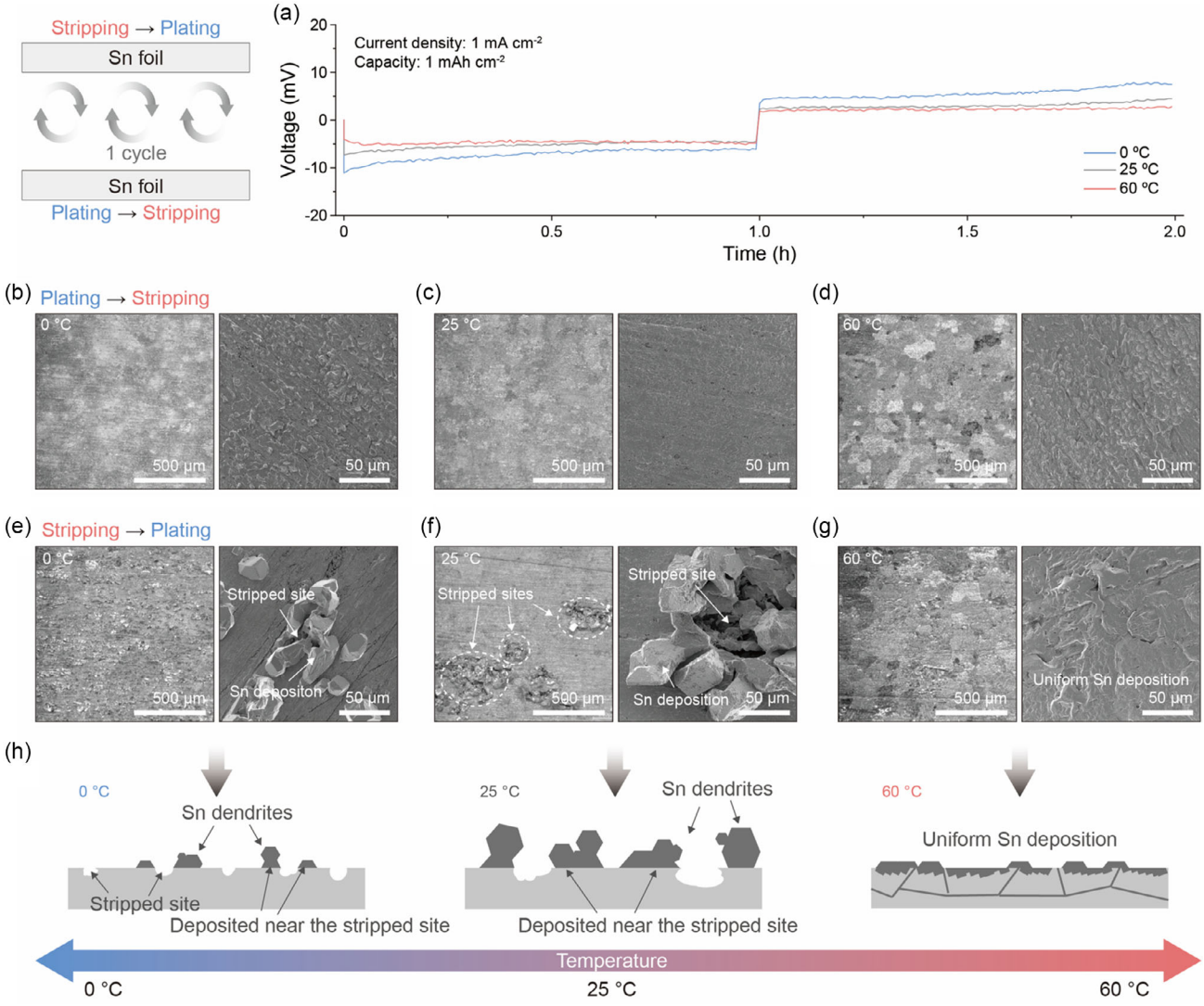

Figure 3. Morphological evolution of Sn electrodes after a complete plating–stripping cycle at various temperatures. a) Voltage profiles of Sn symmetric cells at 0, 25, and 60 °C (1 mA cm^{-2} for 1 mAh cm^{-2}). OM and SEM images of the electrodes after plating followed by stripping at b) 0 °C, c) 25 °C, and d) 60 °C. OM and SEM images of the electrodes after stripping followed by plating at e) 0 °C, f) 25 °C, and g) 60 °C. h) Schematic illustration summarizing the temperature-dependent morphological changes of Sn electrodes after a single cycle at a current density of 1 mA cm^{-2}.

concentrations of 0.05 and 0.2 M in 2 M H_2SO_4 were compared against the reference 0.1 M $SnSO_4$ electrolyte. Additionally, an electrolyte comprising 1 M $Sn(MSA)_2$ and 3 M MSA was employed to investigate anion-related effects. MSA-based electrolyte has been reported to suppress the Sn^{2+}/Sn redox kinetics through coordination between Sn^{2+} and the methanesulfonate anion, which facilitates uniform and fine-grained deposition.[35] Variations in $SnSO_4$ concentration from 0.05 to 0.2 M resulted in surface morphologies similar to those previously observed at 0.1 M, exhibiting consistent temperature-dependent trends (Figure S9a–d, Supporting Information). Although dendrite formation and pit distribution varied slightly depending on concentration, lower temperatures consistently promoted smaller, more widespread dendrites, while elevated temperatures led to uniform Sn deposits devoid of dendritic structures. In the case of the MSA-based electrolyte, finer and more uniformly distributed Sn particles were observed compared to those formed in $SnSO_4$ electrolytes, likely due to coordination interactions between Sn^{2+} ions and methanesulfonate anions (Figure S9e,f, Supporting Information). Despite variations in particle size and distribution, the temperature-dependent behavior remained consistent with that observed in $SnSO_4$-based electrolytes. Finer dendritic structures were formed at lower temperatures, whereas more uniform Sn deposits were obtained at elevated temperatures. Consequently, regardless of variations in electrolyte composition or concentration, the plating and stripping behaviors of Sn electrodes were primarily dictated by temperature-induced kinetic factors. These findings confirm that temperature plays a dominant role in controlling the electrochemical deposition and dissolution processes of Sn.

To further elucidate the temperature-dependent surface behavior of Sn electrodes, additional electrochemical measurements were carried out. Linear sweep voltammetry (LSV) was performed using Sn foil and Ti foil electrodes at 0, 25, and 60 °C

(**Figure 4**a). The results showed that the overpotential was highest at 0 °C, followed by 25 and 60 °C, indicating that the hydrogen evolution reaction is suppressed at lower temperatures. This trend is consistent with the earlier observation that the overpotential required for nucleation decreases as temperature increases. Furthermore, as presented in Figure 4b, the corrosion potential showed a gradual increase with rising temperature and was measured to be 18.5, 20.5, and 21.6 mV for 0, 25, and 60 °C, respectively. In parallel, the corrosion current density increased as the temperature rose, reflecting an acceleration of the corrosion process under thermal influence. This trend aligns with temperature-dependent electrochemical kinetics, where higher thermal energy promotes charge-transfer reactions at the electrode–electrolyte interface by reducing the activation energy. The increase in current density suggests a higher anodic dissolution rate of Sn. This behavior is likely driven by enhanced electron transfer kinetics and improved ionic conductivity at elevated temperatures. These results underscore the role of thermal activation in facilitating surface corrosion processes. To complement the Tafel analysis, cyclic voltammetry (CV) was performed to assess how the electrochemical reaction kinetics vary with temperature. The current response near the onset potential region, which reflects charge-transfer activity at the electrode interface, became progressively steeper as the temperature increased (Figure S10, Supporting Information). Quantitatively, the slopes at 0, 25, and 60 °C were determined to be 0.21, 0.28, and 1.33 mA cm^{-2} mV^{-1}, respectively. This temperature dependence suggests that higher thermal energy enhances both ionic mobility and interfacial electron transfer, resulting in faster reaction rates. The substantial increase observed at 60 °C reinforces the conclusion that elevated temperatures significantly facilitate corrosion-related electrochemical processes.[36] To evaluate corrosion behavior under practical conditions, Sn electrodes were immersed in electrolyte and stored at 0, 25, and 60 °C for a duration of 7 days. As shown in Figure 4c, the electrolyte remained unchanged at 0 and 25 °C. At 60 °C, the electrolyte exhibited a distinct color change, shifting from a clear solution to bright yellow, indicating thermal degradation. This distinct color change indicates that Sn^{2+} ions dissolved in the electrolyte undergo oxidation to Sn^{4+} ions. As a direct result of this oxidation process, Sn^{4+} ions subsequently react within the electrolyte to form SnO_2. The overall oxidation reactions occurring at 60 °C can be described by the following equations.[35]

$$2Sn^{2+} + O_2 + 4H^+ \rightarrow 2Sn^{4+} + 2H_2O \quad (1)$$

$$Sn^{4+} + 2H_2O \rightarrow SnO_2 + 4H^+ \quad (2)$$

The generation of SnO_2 decreases the concentration of electrochemically active Sn^{2+} ions. Consequently, the decreased concentration of Sn^{2+} ions in the electrolyte leads directly to reduced utilization efficiency of the active material, manifesting as a lower Coulombic efficiency and diminished electrochemical performance. Furthermore, the electrodes after the corrosion test showed the formation of nonuniform pits at 60 °C due to severe corrosion, whereas no such pits were observed at 0 and 25 °C (Figure 4d). At low temperatures, stripping induces uneven pit formation on the electrode surface, which subsequently acts as preferential nucleation sites for dendrite growth during plating. In contrast, high temperature accelerates corrosion, leading to the formation of nonuniform pits on the electrode surface. In addition, the electrolyte is rapidly oxidized from Sn^{2+} to Sn^{4+} at high temperature, resulting in the precipitation of SnO_2 (**Figure 5**). Overcoming these challenges is crucial for the development of high-performance ASIBs capable of operating under a wide range of temperatures.

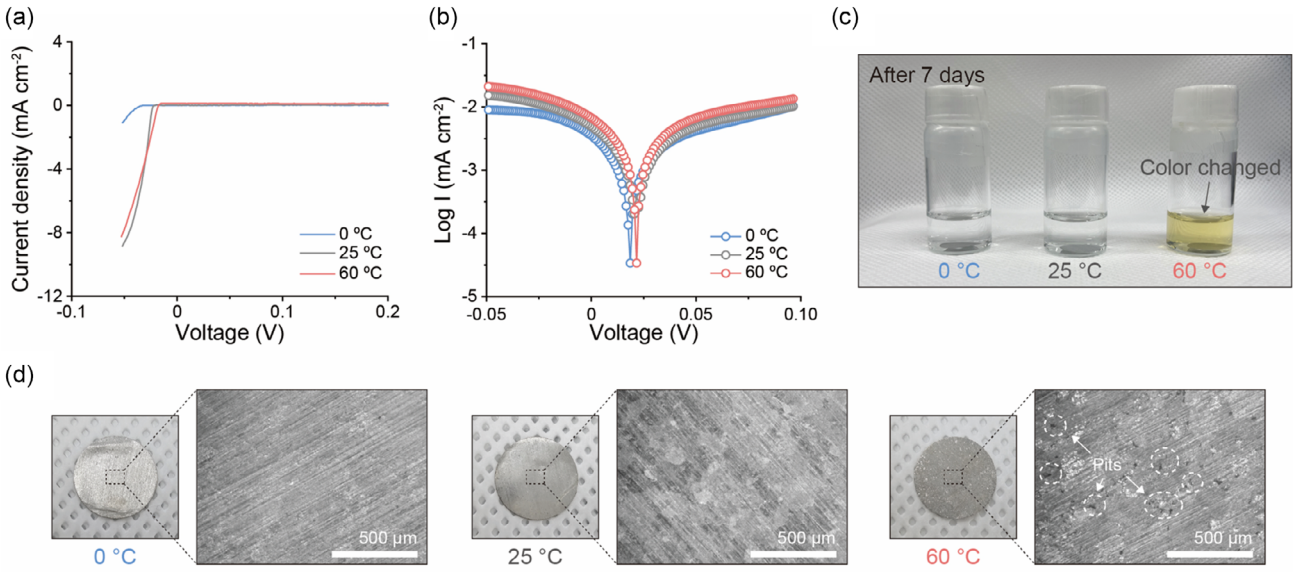

Figure 4. Temperature-dependent corrosion characteristics. a) LSV curves at 0 °C, 25 °C, and 60 °C at scan rate of 2 mV s^{-1}. b) Tafel plots of Sn symmetric cells in 0.1 M $SnSO_4$ electrolyte at different temperatures. c) Photograph of electrolytes after 7 days of corrosion test. d) Photographs and OM images of electrodes after 7 days of corrosion test.

Research Article
doi.org/10.1002/batt.202500230
Chemistry Europe
European Chemical Societies Publishing

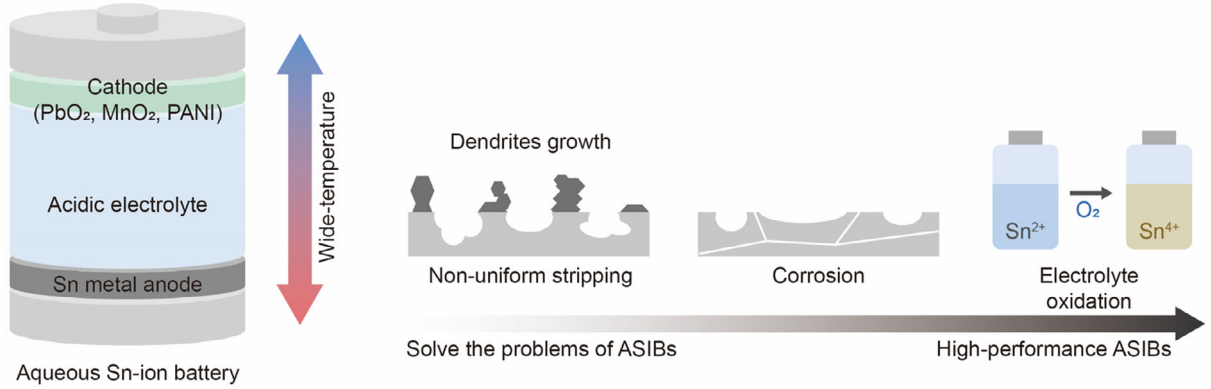

Figure 5. Schematic illustration of ASIBs and their key challenges at different temperatures.

3. Conclusion

Achieving commercial viability for ASIBs requires stable performance over a wide temperature range, necessitating a comprehensive understanding of their temperature-dependent electrochemical behavior. In this study, the surface morphology of Sn electrodes during plating and stripping was investigated at 0, 25, and 60 °C. At 0 °C, reduced ion mobility led to the formation of nonuniform pits on the electrode surface during stripping. During subsequent plating, Sn preferentially deposited around these pits, facilitating dendrite growth. The effect of current density was also significant, with higher current densities intensifying dendrite formation, especially at the electrode edges, thereby increasing the risk of short-circuiting and performance degradation. At 25 °C, stripping resulted in the formation of large pits. Under low current densities, the pits extended deeply into the electrode, whereas at higher current densities, the pits became shallower and wider. The plated surface exhibited polyhedral particle formation, while dendrite growth was observed at the electrode edges. At 60 °C, stripping proceeded uniformly via a layer-by-layer mechanism along grain boundaries and grain surfaces. Subsequent plating onto these uniformly stripped electrodes resulted in uniform Sn deposition, effectively suppressing dendrite formation. However, at high temperatures, corrosion became a significant challenge. Both the corrosion potential and current increased with temperature, accelerating the corrosion process and leading to pit formation on the electrode surface. This study provides a comprehensive analysis of the temperature-dependent stripping, plating, and corrosion behaviors of Sn electrodes. The results highlight key factors that govern interfacial stability and morphological evolution, which are critical for improving the reversibility of Sn metal anodes in ASIBs. By clarifying the conditions required for uniform electrochemical behavior over a wide temperature range, this work offers meaningful guidance for the design of ASIBs intended for use in environments with frequent thermal fluctuations, such as large-scale ESS. These findings contribute to a deeper understanding of temperature-sensitive electrochemical processes, which is essential for ensuring reliable operation under practical conditions.

4. Experimental Section

Electrodes and Electrolyte Preparation

Sn foil (0.05 mm, Goodfellow) was polished with sandpaper to remove the surface oxide layer and then sequentially cleaned with acetone and ethanol. For electrochemical analysis using beaker cells, Sn and Ti foils were cut into rectangular pieces (1 cm × 3.5 cm). Kapton tape was applied to the Sn foil for insulation, leaving an exposed electrode area of 1 cm × 1 cm for electrochemical reactions. To fabricate coin cells, CR-2032 coin cells with Sn foils, glass fiber separator (Whatman GF/A), and 100 μL of electrolyte were used. The diameters of the Sn foil and glass fiber were 14 and 19 mm, respectively. The electrolyte solution was prepared by dissolving 0.05, 0.1, and 0.2 M $SnSO_4$ in a 2 M H_2SO_4 aqueous solution. In addition, an MSA-based electrolyte composed of 1 M $Sn(MSA)_2$ and 3 M MSA was prepared. All chemicals were purchased from Sigma-Aldrich and used as received without further purification.

Electrochemical Measurement

Electrochemical measurements were conducted in a symmetric beaker-cell configuration using four different electrolyte compositions. Each electrolyte was placed in a separate beaker cell, and Sn electrodes, insulated with Kapton tape to define an active area of 1 cm^2, were employed as both working and counter electrodes. Experiments were conducted under two different current density conditions, at 1 mA cm^{-2} for 1 mAh cm^{-2} and at 10 mA cm^{-2} for 1 mAh cm^{-2}. For additional electrochemical characterization, LSV was conducted using an Sn electrode and a Ti electrode with a ZIVE SP1 (Wonatech) instrument. The CV was conducted using Sn electrode at a scanning rate of 50 mV s^{-1}. The Sn//Sn symmetric coin cells were used to test the long-term cycling performance. Corrosion tests were performed by placing 0.1 M $SnSO_4$, immersing Sn electrodes, and storing at 0, 25, and 60 °C for 7 days.

Material Characterizations

The surface morphology of the Sn electrodes was examined using an OM, and digital images were captured for further evaluation. For more detailed surface characterization, SEM (SUPRA 55VP, Zeiss) was used. The crystalline structure of the electrodes was examined using XRD (JP/D/MAX-2500H, Rigaku) using a Cu K_α radiation source.

Acknowledgements

Y.-H.L. and H.A. contributed equally to this work. This work was supported by the National Research Foundation of Korea (NRF) grant funded by the Korea Government (MSIT) (RS-2025-00518953) and the National Research Foundation of Korea (NRF) grant funded by the Korea Government (MSIT) (RS-2024-00422387). This study was also supported by the Institute for Basic Science (project code: IBS-R006-A2).

Conflict of Interest

The authors declare no conflict of interest.

Data Availability Statement

The data that support the findings of this study are available in the supplementary material of this article.

Keywords: aqueous batteries · aqueous Sn-ion batteries · Sn metals · surface morphologies · temperature dependent

[1] K. Liu, Y. Liu, D. Lin, A. Pei, Y. Cui, *Sci. Adv.* **2018**, *4*, eaas9820.
[2] Y. Wang, D. Zhou, V. Palomares, D. Shanmukaraj, B. Sun, X. Tang, C. Wang, M. Armand, T. Rojo, G. Wang, *Energy Environ. Sci.* **2020**, *13*, 3848.
[3] S. Yuan, K. Ding, X. Zeng, D. Bin, Y. Zhang, P. Dong, Y. Wang, *Adv. Mater.* **2023**, *35*, 2206228.
[4] J. Hao, X. Li, X. Zeng, D. Li, J. Mao, Z. Guo, *Energy Environ. Sci.* **2020**, *13*, 3917.
[5] Y.-H. Lee, Y. Jeoun, S.-H. Lee, J. H. Kim, S.-Y. Kim, S.-H. Yu, K.-S. Ahn, Y.-E. Sung, *Chem. Eng. J.* **2023**, *464*, 142580.
[6] B. K. Cho, S. H. Huh, S. H. Kim, S. Yu, J. S. Bae, J. K. Yoo, S. H. Yu, *Carbon Energy* **2024**, *6*, e441.
[7] D. Chao, W. Zhou, C. Ye, Q. Zhang, Y. Chen, L. Gu, K. Davey, S. Z. Qiao, *Angew. Chem.* **2019**, *131*, 7905.
[8] M. Kim, H. Kim, S.-H. Lee, S. Yu, W. Kim, J.-S. Bae, C.-Y. Ahn, H. Shim, J. E. Lee, S.-H. Yu, *Chem. Eng. J.* **2024**, *481*, 148256.
[9] Y. H. Lee, Y. Jeoun, J. H. Kim, J. Shim, K. S. Ahn, S. H. Yu, Y. E. Sung, *Adv. Funct. Mater.* **2024**, *34*, 2310884.
[10] H. Zhang, D. Xu, F. Yang, J. Xie, Q. Liu, D.-J. Liu, M. Zhang, X. Lu, Y. S. Meng, *Joule* **2023**, *7*, 971.
[11] S.-H. Huh, Y. J. Choi, S. H. Kim, J.-S. Bae, S.-H. Lee, S.-H. Yu, *J. Mater. Chem. A* **2023**, *11*, 19384.
[12] H. Zhou, Q. Kuang, J. Li, Y. Jin, Y. Li, Q. Fan, Y. Dong, Y. Zhao, *Small* **2024**, *20*, 2404215.
[13] Y. Li, Z. Cui, L. Zhang, B. Yan, H. Tao, X. Yang, *Adv. Funct. Mater.* **2025**, 2424582.
[14] H. Zhang, D. J. Liu, K. Xu, Y. S. Meng, *Adv. Mater.* **2025**, 2417757.
[15] Q. Nian, T. Sun, S. Liu, H. Du, X. Ren, Z. Tao, *Chem. Eng. J.* **2021**, *423*, 130253.
[16] M. Chen, S. Xie, X. Zhao, W. Zhou, Y. Li, J. Zhang, Z. Chen, D. Chao, *Energy Storage Mater.* **2022**, *51*, 683.
[17] Z. Ma, J. Chen, J. Vatamanu, O. Borodin, D. Bedrov, X. Zhou, W. Zhang, W. Li, K. Xu, L. Xing, *Energy Stor. Mater.* **2022**, *45*, 903.
[18] L. Jiang, D. Dong, Y.-C. Lu, *Nano Res. Energy* **2022**, *1*, e9120003.
[19] M. S. Ding, A. von Cresce, K. Xu, *J. Phys. Chem. C* **2017**, *121*, 2149.
[20] J. Wang, Y. Yang, Y. Wang, S. Dong, L. Cheng, Y. Li, Z. Wang, L. Trabzon, H. Wang, *ACS nano* **2022**, *16*, 15770.
[21] E. R. Cooper, M. Li, I. Gentle, Q. Xia, R. Knibbe, *Angew. Chem.* **2023**, *135*, e202309247.
[22] Q. Ma, R. Gao, Y. Liu, H. Dou, Y. Zheng, T. Or, L. Yang, Q. Li, Q. Cu, R. Feng, *Adv. Mater.* **2022**, *34*, 2207344.
[23] J. Su, X. Yin, H. Zhao, H. Yang, D. Yang, L. He, M. Wang, S. Jin, K. Zhao, Y. Wang, *Nano Lett.* **2022**, *22*, 1549.
[24] Y. Sun, B. Liu, L. Liu, X. Yan, *Adv. Funct. Mater.* **2022**, *32*, 2109568.
[25] M. Han, T. C. Li, X. Chen, H. Y. Yang, *Small* **2024**, *20*, 2304901.
[26] J. Zhang, Z. Liu, Y. Zhang, N. Zhang, *Chem. Eng. J.* **2025**, *506*, 160157.
[27] H. Zhang, L. Yang, H. Wang, B. Cui, J. Wang, X. Han, W. Hu, *Adv. Funct. Mater.* **2024**, *34*, 2312469.
[28] Y. Yao, Z. Wang, Z. Li, Y. C. Lu, *Adv. Mater.* **2021**, *33*, 2008095.
[29] Y. Zhao, S. Guo, M. Chen, B. Lu, X. Zhang, S. Liang, J. Zhou, *Nat. Commun.* **2023**, *14*, 7080.
[30] X. Feng, P. Li, J. Yin, Z. Gan, Y. Gao, M. Li, Y. Cheng, X. Xu, Y. Su, S. Ding, *ACS Energy Lett.* **2023**, *8*, 1192.
[31] P. Zou, R. Zhang, L. Yao, J. Qin, K. Kisslinger, H. Zhuang, H. L. Xin, *Adv. Energy Mater.* **2021**, *11*, 2100982.
[32] C. D. Owen, M. Grant Norton, *J. Mater. Sci.* **2016**, *51*, 577.
[33] R. Failla, M. Bologna, B. Tellini, *J. Power Sources* **2019**, *433*, 126675.
[34] L. Gireaud, S. Grugeon, S. Laruelle, B. Yrieix, J.-M. Tarascon, *Electrochem. Commun.* **2006**, *8*, 1639.
[35] Q. Wang, F. Zhang, Y. Shu, H. Xiao, X. Zhang, X. Ma, J. Liu, Y. Wang, J. Huang, Y. Xia, *Angew. Chem.* **2025**, *137*, e202418928.
[36] M. Cardoso, S. Amaral, E. Martini, *Corros. Sci.* **2008**, *50*, 2429.

Manuscript received: March 26, 2025
Revised manuscript received: May 13, 2025
Version of record online: